Topological edge modes by smart patterning

David J. Apigo,[1] Kai Qian,[1] Camelia Prodan,[1] and Emil Prodan[2]
[1]*Department of Physics, New Jersey Institute of Technology, Newark, New Jersey 07102, USA*
[2]*Department of Physics, Yeshiva University, New York, New York 10016, USA*

(Received 22 August 2018; published 20 December 2018)

We study identical coupled mechanical resonators whose collective dynamics are fully determined by the patterns in which they are arranged. In this work, we call a system topological if (1) boundary resonant modes fully fill all existing spectral gaps whenever the system is halved, and (2) if the boundary spectrum cannot be removed or gapped by any boundary condition. We demonstrate that such topological characteristics can be induced solely through patterning, in a manner entirely independent of the structure of the resonators and the details of the couplings. The existence of such patterns is proven using K theory and exemplified using an experimental platform based on magnetically coupled spinners. Topological metamaterials built on these principles can be easily engineered at any scale, providing a practical platform for applications and devices.

DOI: 10.1103/PhysRevMaterials.2.124203

I. INTRODUCTION

Experimental demonstrations of topological effects in classical mechanical systems abound [1–24] and the field is rapidly moving towards the next stage, where practical devices and concrete applications ought to emerge. However, it is extremely difficult to maintain control over the designs as the systems are scaled down to meet certain practical constraints, especially those based on specific configurations and values of the couplings. In this work, we demonstrate that topological boundary modes can emerge solely from a smart patterning of a metamaterial. More precisely, metamaterials made out of bundles or stacks of certain patterns have all their bulk spectral gaps completely filled with topological edge spectrum when the system is halved. This edge spectrum cannot be gapped by any boundary condition or by adiabatic deformation of the metamaterial. The phenomenon is completely due to the patterning and does not require any tuning of the couplings, except for the opening of gaps in the bulk resonant vibrational spectrum. Due to such minimal tuning, metamaterials designed on these principles may be fabricated at any scale, hence providing a viable pathway towards concrete practical applications.

The goal of our paper is twofold: On one hand, we seek to demonstrate the experimental manifestation of the topological boundary modes in one such smartly patterned metamaterial and, on the other hand, we want to explain the theoretical principles behind these unusual predictions. For the first part, we introduce an experimental platform based on magnetically coupled spinners. Its hallmark feature is that arbitrarily complex mechanical resonators and couplings can be built by engineering one degree of freedom at a time (see Sec. II). The experimental platform not only enables the realization and characterization of a topological pattern of mechanical resonators, but also helps with the formulation and exemplification of the theoretical concepts, which otherwise may appear quite abstract. Indeed, such topological patterns are necessarily aperiodic, thus the traditional Bloch-Floquet analysis is unavailable. The natural theoretical tool to use in such situations is the K theory of C^* algebras, as introduced in the pioneering works of [25] and [26]. Based on this formalism, we formulate a K-theoretic bulk-boundary principle for generically patterned resonators. This principle enables one to resolve the precise conditions in which the topological edge spectrum emerges as well as the mechanism behind this phenomenon. Prediction of topological patterns then becomes routine. For simplicity, the present study is restricted to one-dimensional patterns but generalizations to higher dimensions can be easily achieved based on [27] (see, e.g., [28]). Let us point out that the effect of a magnetic field can be also incorporated in the analysis [29].

We believe these theoretical methods of analysis would be extremely useful additions to the materials scientist toolbox and we think that, by combining the somewhat abstract concepts with the concrete experiments, we have finally found a formula to explain the framework to a broad scientific community.

The paper is organized as follows. In Sec. II, the experimental platform based on magnetically coupled spinners is introduced. In particular, we show how to quantitatively map the coupling functions and how to obtain the dynamical matrices that drive the dynamics of the collective resonant modes when the spinners are assembled in arbitrary patterns. This concrete setting is used to explain what topological classification over a fixed pattern means and to give the first hints to why such a program is feasible, despite the fact that the pattern can be arbitrary. In particular, using elementary calculations, we demonstrate that all dynamical matrices take a very specific form, involving only a small set of operators. This leads us in Sec. III to introduce the algebra of bulk physical algebras, which generates all possible dynamical matrices over a pattern via a canonical representation. For the proposed patterns, this algebra is computed explicitly and shown to be isomorphic to the algebra generated by magnetic translations. Section IV illustrates the bulk spectra of the proposed patterns and points to the similarity with the Hofstadter butterfly [30]. We also

illustrate the good agreement between numerical and experimental mappings of the spectra. A review of Bellissard's gap labeling procedure [31] is used to rationalize the complexity of the spectra and we show how to compute bulk topological invariants solely from the integrated density of states. It is at this point where the K theory is introduced. Section V is dedicated to the edge analysis. We illustrate the manifestation of the topological edge spectrum through both numerical simulations and quantitative experimental measurements as well as video recordings. Additionally, we explain the K-theoretic bulk-boundary mechanism, which culminates with the proof that, indeed, the proposed patterns are topological. A discussion of possible applications concludes the exposition.

Last, let us relate our work with the existing literature. The emergence of the topological boundary spectrum in quasiperiodic structures was pointed out theoretically and observed experimentally in [32,33]. Questions about these systems were raised in [34], namely, were the topological characteristics noted in [32] a property of one pattern or of an ensemble of patterns? Reference [35] provided answers using some of the algebraic methods employed in the present work. By passing from numerical topological invariants to the K-theory groups, we answer those questions completely while providing a global chart of all possible topological systems over a quasiperiodic pattern. Additionally, we provide experimental observation of such topological edge modes in a quasiperiodic mechanical system. The authors emphasize that this work is part of the vigorous effort of the metamaterials community on the search for topological boundary resonances in aperiodic systems [32–52]. This exploration goes well beyond the periodic table of topological insulators and superconductors [53–55].

II. MAGNETICALLY COUPLED SPINNERS: A VERSATILE EXPERIMENTAL PLATFORM

Utilizing an experimental platform which can be easily reconfigured and quantitatively characterized enables one to engineer patterns of coupled mechanical resonators with predefined internal structures and couplings, and to study the spectral properties of virtually any imaginable discrete model. The experimental control over these systems is extremely high, resulting in excellent agreement between theory and experiment. One particular configuration is discussed in detail to exemplify the experimental procedures and is used to demonstrate a topological pattern. The experimental platform will also be used to introduce the program of topological classification over an aperiodic pattern and other more abstract concepts.

A. Coupling and dynamics

A configurable spinner is illustrated in Fig. 1(a). It consists of a stainless-steel ball bearing mounted in a threaded brass encapsulation. This enables the spinners to be adorned with a multitude of components. The centers of the spinners are pinned down, resulting in one rotational degree of freedom φ. By stacking and coupling such spinners, extremely complex systems can be built one degree of freedom at time [illustrated in Fig. 1(b)]. With full control over the degrees of freedom and

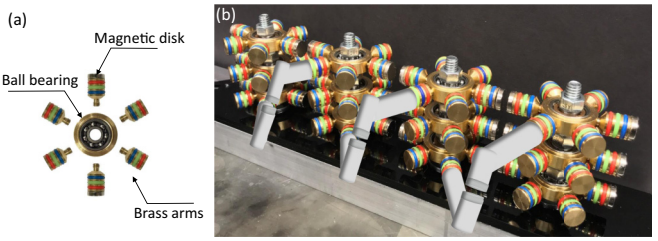

FIG. 1. Magnetically coupled spinners: A versatile experimental platform. (a) Example of the basic spinner configuration used in the present work. The arms are detachable such that the spinners can be easily refitted. (b) Exemplification of a relative complex linear configuration of coupled spinners, with coupling in front sideways (shown) and in the back (not shown).

couplings, any quadratic Hamiltonian can be implemented to drive the small oscillations of the coupled spinners. For example, using this very platform, the generators of the entire classification table of topological condensed-matter systems have been recently implemented with passive metamaterials in [56].

The present work features a spinner with six grooved indentations and with heavy brass arms securely fastened in the brass encapsulation. Two of the arms are fitted with neodymium magnetic disks, which provide the couplings between each spinner when arranged in linear patterns. These magnetic couplings can be measured by mapping the resonant modes of a dimer, whose dynamics is governed by the Lagrangian (I = moment of inertia):

$$L(\varphi_1, \varphi_2, \dot{\varphi}_1, \dot{\varphi}_2) = \tfrac{1}{2} I \dot{\varphi}_1^2 + \tfrac{1}{2} I \dot{\varphi}_2^2 - V(\varphi_1, \varphi_2). \quad (1)$$

In the regime of small oscillations around the equilibrium configuration $\varphi_1 = \varphi_2 = 0$, the potential can be approximated quadratically:

$$V(\varphi_1, \varphi_2) = \tfrac{1}{2}\alpha\left(\varphi_1^2 + \varphi_2^2\right) + \beta\varphi_1\varphi_2, \quad (2)$$

and the pair of the two resonant modes can be computed explicitly:

$$f_\pm = \sqrt{\frac{\alpha \pm \beta}{4\pi^2 I}}. \quad (3)$$

The measured resonant frequencies are reported in Fig. 2 as functions of distance d between the magnets. Equations (3) can be inverted:

$$\alpha = 2\pi^2 I\,(f_+^2 + f_-^2), \quad \beta = 2\pi^2 I\,(f_+^2 - f_-^2), \quad (4)$$

which, together with the experimental data, enables us to determine the functional dependencies $\alpha(d)$ and $\beta(d)$ of the coupling coefficients. The details are provided in Fig. 2 and note that units of $2\pi^2 I$ are used henceforth for the coupling functions. The functional dependencies are well fitted by

$$\alpha(d) = -\frac{654.09}{\sqrt{d}} + \frac{2763.66}{d} + \frac{575.89}{d^2},$$
$$\beta(d) = -\frac{778.14}{\sqrt{d}} + \frac{3439.81}{d} + \frac{161.35}{d^2}. \quad (5)$$

When the centers of the spinners are pinned in a one-dimensional pattern $\omega = \{x_n\}_{n\in\mathbb{Z}}$, the Lagrangian of the

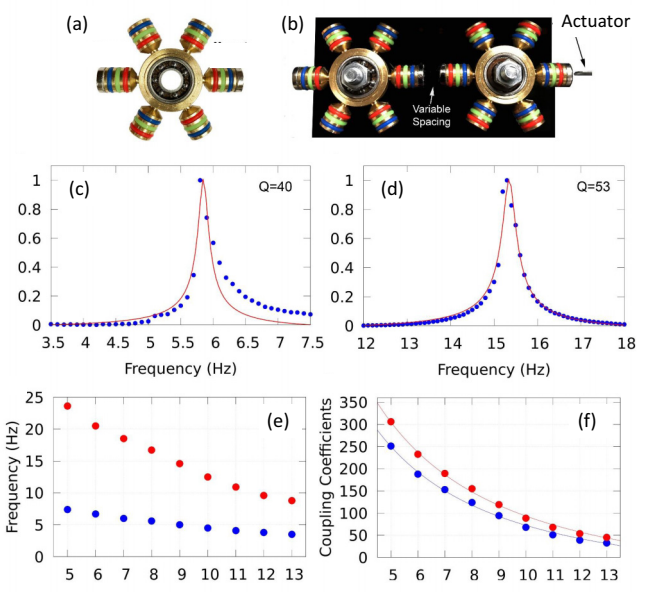

FIG. 2. Mapping the coupling coefficients. (a) Illustration of a single spinner with the locations of magnets indicated. (b) Experimental apparatus for measuring the interaction potential of a dimer. Two spinners are placed on an aluminum track with variable distance d. The system is actuated and the response is recorded using accelerometers. (c),(d) Response of the coupled spinner as the frequency is swept over the low and high resonances of dimers spaced 9 mm apart. The standard fits indicate quality factors of $Q = 40,\ 53$, respectively. (e) Map of the high (red) and low (blue) resonant frequencies as functions of magnet spacing. (f) The coupling functions α (red dots) and β (blue dots), as derived from (4) and the data from panel (e), together with the fit functions from Eqs. (5).

system becomes

$$L = \sum_{n\in\mathbb{Z}} \left[\frac{1}{2} I \dot{\varphi}_n^2 - (\alpha(d_n - 1) + \alpha(d_n))\varphi_n^2 - \beta(d_n)\varphi_n\varphi_{n+1} \right], \tag{6}$$

where $d_n = x_{n+1} - x_n - D$ with D the diameter of a spinner. The equations of motion read

$$-I\ddot{\varphi}_n = [\alpha(d_{n-1}) + \alpha(d_n)]\varphi_n + \beta(d_{n-1})\varphi_{n-1} + \beta(d_n)\varphi_{n+1}. \tag{7}$$

The degrees of freedom can be encoded in the column vector:

$$|\varphi\rangle = (\ldots, \varphi_{-1}, \varphi_0, \varphi_1, \ldots)^T, \tag{8}$$

and let us denote by $|n\rangle$ the column vector with 1 at position n and 0 in the rest. Then $|\varphi\rangle = \sum_n \varphi_n |n\rangle$ and, with the ansatz $|\varphi(t)\rangle = \mathrm{Re}[e^{i2\pi ft}|\psi\rangle]$ and the units from Fig. 2, the system of equations of motion becomes $f^2|\psi\rangle = H|\psi\rangle$ with

$$H = \sum_{n\in\mathbb{Z}} \{[\alpha(d_{n-1}) + \alpha(d_n)]|n\rangle\langle n| + \beta(d_{n-1})|n\rangle\langle n-1| + \beta(d_n)|n\rangle\langle n+1|\}. \tag{9}$$

It is now a classical eigensystem for the Hamiltonian H in the Hilbert space $\ell^2(\mathbb{Z})$.

We present this analysis in detail because it serves as a model for generically patterned resonators. For example, it can be implemented for other spinner configurations, even for complex ones that include stacking and couplings beyond nearest neighbors. Throughout this paper, especially when discussing continuous deformations of the systems, it is extremely helpful to have a physical realization in mind.

B. Aperiodic yet fully classifiable

To resolve the bulk-boundary correspondence principle for these systems, one must deal with the classification of gapped bulk Hamiltonians over the pattern ω. To properly define the pattern, recall that the spinners can be easily reconfigured, hence the Hamiltonian (9) is only one of many that can be implemented over ω. When N spinners are stacked at each point of the pattern, the Hilbert space becomes $\mathbb{C}^N \otimes \ell^2(\mathbb{Z})$, with elementary vectors of the form $\xi \otimes |n\rangle$, and the most general Hamiltonian driving the small oscillations of the coupled spinners takes the form

$$H_\omega = \sum_{n,n'} w_{n,n'}(\omega) \otimes |n\rangle\langle n'|, \tag{10}$$

where $w_{n,n'} \in M_N(\mathbb{C})$ with $w_{n',n} = w_{n,n'}^\dagger$. Throughout, $M_N(\mathbb{C})$ denotes the space of $N \times N$ matrices with complex entries. The above expression allows couplings beyond the first nearest neighbors and allows for the coupling $N \times N$ matrices to depend on arbitrarily many geometrical data from the pattern ω. The coupling coefficients can be changed continuously (e.g., by modifying the strength of the magnets). Furthermore, by stacking a large number of spinners on top of each other at each point of the pattern, one can smoothly activate or deactivate internal degrees of freedom, changing the dimension N. These will be the allowed continuous deformations of our physical systems. It is useful to view a gapped Hamiltonian as a pair (H_ω, G), where G is a connected component of the resolvent set $\mathbb{R} \setminus \mathrm{Spec}(H_\omega)$. Two gapped Hamiltonians (H_ω, G) and (H'_ω, G') are said to be in the same topological class if a continuous gapped deformation connecting the two Hamiltonians exists. The topological classification of the gapped Hamiltonians consists of enumerating these topological classes as well as spelling out at least one representative for each class.

Considering generic aperiodic patterns, the topological classification may appear a daunting task. To understand why this classification is achievable, several key observations are in place:

(1) The pattern ω needs to be treated as an ordinary variable. It takes values in the space of point patterns, a space that can be characterized and topologized using procedures that by now are quite standard [57]. Existence of a topology is important in defining what a continuous deformation of a point pattern is.

(2) Since the spinners are identical copies of a basic design, once the internal structure of the basic spinner is set, the functional dependencies of the couplings on ω are fixed. More precisely, if the pattern is changed to ω', we will use the same functions $w_{n,n'}$ but evaluate them at ω'.

(3) Per previous observation, a better terminology for the coupling coefficients would be coupling functions. This is a useful concept because ω, as a point in the space of patterns, contains all the geometric information of the pattern. In

general, the coupling coefficients depend on many geometric details of the pattern. If the concept of coupling functions is adopted, then those complicated dependencies can be written concisely as $w_{n,n'}(\omega)$.

(4) The coupling functions are assumed to be continuous of ω. We will also consider cases where $w_{n,n'}(\omega)$ becomes negligible for n and n' far apart. Both assumptions are usually met in practice.

The particular Hamiltonian (9) reflects all these principles, through the fact that $\alpha(d)$ and $\beta(d)$ have been measured once and then properly evaluated and applied to the arbitrary pattern ω. The analysis and the measurements that led to (9) can be repeated for more complex spinner structures and couplings, and the principles will emerge again. While they seem obvious, these observations bring a unique perspective, which is key to solving the topological classification.

Gearing towards that solution, note the natural action of the $\mathbb{Z}$ group on the space of one-dimensional patterns:

$$\mathbb{Z} \ni a \to \tau_a\omega = \tau_a\{x_n\}_{n\in\mathbb{Z}} = \{x_{n+a} - x_a\}_{n\in\mathbb{Z}}. \tag{11}$$

We will always fix the point labeled by 0 at the origin of the real axis and set the labels to be consistent with the ordering $\cdots < x_{-1} < x_0 = 0 < x_1 < \cdots$. This implicitly assumes that two points are never on top of each other. Then τ_a can be identified with the rigid translation of the pattern that brings point x_a at the origin. Galilean symmetry requires that

$$w_{n-a,n'-a}(\tau_a\omega) = w_{n,n'}(\omega) \Rightarrow w_{n,n'}(\omega) = w_{0,n'-n}(\tau_n\omega). \tag{12}$$

Dropping one redundant index and using $q = n' - n$, as well as the shift operator,

$$S|n\rangle = |n-1\rangle, \quad S^\dagger|n\rangle = |n+1\rangle, \quad SS^\dagger = S^\dagger S = I, \tag{13}$$

the generic Hamiltonian takes the form

$$H_\omega = \sum_q \sum_n w_q(\tau_n\omega) \otimes |n\rangle\langle n|\, S^q. \tag{14}$$

This expression already reveals a very particular structure. Also, in order to reproduce H_ω, one only needs to evaluate the coupling functions on a small subset of the space of patterns, namely

$$\Xi = \overline{\{\tau_n\omega,\ n \in \mathbb{Z}\}}, \tag{15}$$

where the overline indicates the topological closure of the otherwise discrete set of translated patterns. In the professional literature [57], the tuple (Ξ, τ), which is a bona fide topological dynamical system, is called the discrete hull of the pattern. A system is called homogeneous if the orbit $\{\tau_n\omega'\}_{n\in\mathbb{Z}}$ is dense in Ξ for any pattern $\omega' \in \Xi$. We will be dealing exclusively with homogeneous patterns.

The main conclusion is that every Hamiltonian over the pattern ω can be generated using just the shift operator S and diagonal operators of the form $\sum_n f(\tau_n\omega)|n\rangle\langle n|$ with f a continuous function over Ξ. In many instances, the algebra generated by these operators is very simple and connects to other well-known and well-studied algebras. Ultimately, completing the topological classification program over a point pattern is conditioned by the ability to resolve the topological set Ξ and the action of $\mathbb{Z}$ on it.

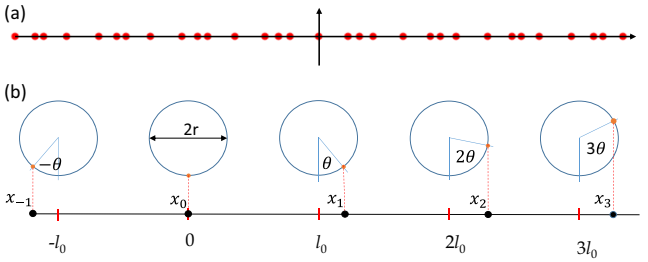

FIG. 3. Example of a pattern with discrete hull equivalent to $\mathbb{S}^1$. (a) Display of a finite number of points of a pattern generated by the algorithm $x_n = n\,l_0 + r\,\sin(n\theta)$, with the particular values $l_0 = 1$, $r = 0.4$, and $\theta = \frac{2\pi}{\sqrt{15}}$. (b) A geometric algorithm to generate the same pattern, revealing that $\Xi \simeq \mathbb{S}^1$.

C. Generating patterns with prescribed hull

Here, we generate a class of patterns for which Ξ is topologically equivalent with the circle $\mathbb{S}^1$. The simplest pattern is illustrated in Fig. 3(a) and it has the analytic expression

$$x_n = n\,l_0 + r\,\sin(n\theta), \quad r < \frac{l_0}{2}, \quad n \in \mathbb{Z}. \tag{16}$$

The geometric algorithm explained in Fig. 3(b) can be used to formally derive that $\Xi \simeq \mathbb{S}^1$. Consider a rigid translation $\tau_a\omega$ of the pattern such that the old x_a now sits at the origin of the real axis. Associated to this x_a there is a point on the circle and it is evident that knowing where this point is located enables us to reproduce the entire translated pattern $\tau_a\omega$. Applying the geometric algorithm described in Fig. 3(b) (starting from angle $a\theta$ instead of 0) establishes a one-to-one relationship between the translated patterns $\tau_a\omega$ and the angles $a\theta$, $a \in \mathbb{Z}$. For θ irrational (in units of 2π), these points densely fill the circle. It is important to note that Ξ is just a topological space and it has no geometry. From a topological point of view, any closed loop is also a circle, hence more complex patterns can be generated by the same algorithm but using a deformed circle. Such a pattern is illustrated in Fig. 4(a). As one can see, although the algorithm is simple, the resulting patterns can be extremely complex and irregular looking. Using the same arguments, one can quickly see that Ξ is just the closed loop traced in Fig. 4(b), hence $\Xi \simeq \mathbb{S}^1$.

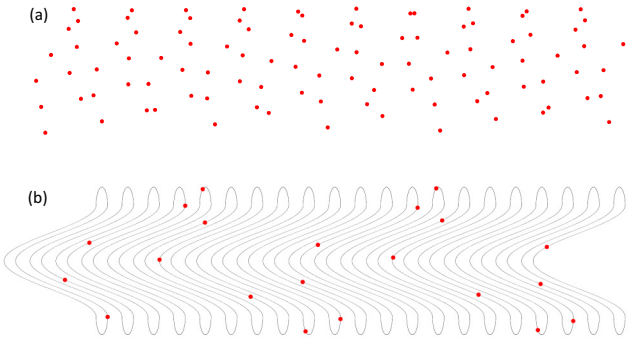

FIG. 4. Additional example of a pattern with discrete hull equivalent to $\mathbb{S}^1$. (a) Display of a finite number of points. (b) The geometric algorithm used to generate the pattern consists of translation by θ along the loop followed by a horizontal translation by one unit.

Based on the above remarks, one can see that we can actually allow not only continuous deformations of the resonators but also of the patterns themselves, provided the topology of the hull remains unchanged. This will be assumed from now on and will be covered by our topological classification.

III. C^*-ALGEBRAIC APPROACH

It is instructive to inspect the commutation relations between the basic operators, which for $N = 1$ are

$$\left(\sum_n f(\tau_n\omega)|n\rangle\langle n|\right)S = S\left(\sum_n f(\tau_n\omega)|n-1\rangle\langle n-1|\right) = S\left(\sum_n f(\tau_{n+1}\omega)|n\rangle\langle n|\right). \tag{17}$$

This demonstrates that, when conjugating the specific diagonal operators by S, f was effectively replaced by $f \circ \tau_1$. This observation enables us to define an abstract algebra which generates all Hamiltonians H_ω for all $\omega \in \Xi$.

A. Algebra of bulk physical observables

We will discuss three important aspects even though some might appear technical at first sight. First is the definition of the algebra $\mathcal{A}$ of bulk physical observables. It is the universal C^* algebra generated by the algebra $C_N(\Xi)$ of continuous function over Ξ with values in $M_N(\mathbb{C})$ and by a unitary operator u ($uu^* = u^*u = 1$), satisfying the commutation relations which stem directly from (17):

$$fu = u(f \circ \tau_1), \quad \forall\, f \in C_N(\Xi). \tag{18}$$

A generic element from this algebra takes the form $a = \sum_q a_q u^q$, where all coefficients a_q are from $C_N(\Xi)$. The canonical representation on $\mathbb{C}^N \otimes \ell^2(\mathbb{Z})$ is provided by

$$C_N(\Xi) \ni f \to \pi_\omega(f) = \sum_n f(\tau_n\omega) \otimes |n\rangle\langle n| \tag{19}$$

and $u \to S$, which we already verified in (17) to respect the commutation relations of $\mathcal{A}$. One can see explicitly that $\pi_\omega(h)$, $h = \sum_q w_q u^q$, generates (14). The algebra $\mathcal{A}$ generates not only the Hamiltonians but all covariant physical observables over the patterns from Ξ, that is, the families of operators $\{A_\omega\}_{\omega\in\Xi}$ with the property

$$S^{-n}A_\omega S^n = A_{\tau_n\omega}, \quad \forall\, \omega \in \Xi. \tag{20}$$

Second, since one of the main themes is the classification under continuous deformations, we need to introduce a norm for $\mathcal{A}$ in order to make precise what the latter means. The canonical norm on $\mathcal{A}$ is

$$\|a\| = \sup_{\omega\in\Xi} \|\pi_\omega(a)\|, \tag{21}$$

where on the right is the ordinary operator norm. When completed under (21), $\mathcal{A}$ becomes a separable C^* algebra, which for our program is extremely important because these algebras have well-defined topological K theories and their K groups are always countable. In other words, we are assured that we have a sensible and useful topological classification.

Third, there is an important relationship between the spectrum of an element $h \in \mathcal{A}$ and the spectra of operators $\pi_\omega(a)$ that stem from it. Recall that the resolvent set of a is

$$\mathrm{Res}(a) = \{\lambda \in \mathbb{C} \mid \lambda - a \text{ is invertible in } \mathcal{A}\}. \tag{22}$$

The spectrum of a is then $\mathrm{Spec}(a) = \mathbb{C} \setminus \mathrm{Res}(a)$, a definition that actually makes sense for an arbitrary algebra. In general, we have the isomorphism

$$\mathcal{A} \simeq \bigoplus_{\omega\in\Xi} \pi_\omega(\mathcal{A}) \Rightarrow \mathrm{Spec}(h) = \bigcup_{\omega\in\Xi} \mathrm{Spec}(H_\omega). \tag{23}$$

However, for a homogeneous system, $\mathrm{Spec}(H_\omega)$ is independent of ω and, as such

$$\mathrm{Spec}(h) = \mathrm{Spec}(H_\omega)\, \forall\, \omega \in \Xi, \tag{24}$$

a conclusion which will play an important role in our final discussion.

B. Explicit computations

If the pattern ω is periodic, then Ξ is a point and the algebra $\mathcal{A}$ is generated by the shift operator S. Hence, it is commutative and we are dealing with the ordinary band theory.

If ω is a disordered lattice, i.e., small random displacements drawn from the interval $[-r, r]$ of otherwise equally spaced points, then Ξ is the Hilbert cube $[-r, r]^{\mathbb{Z}}$. This space has trivial topology since it is contractible to a point and the K theory of the resulting observable algebra is the same as the K theory of the periodic lattice [27].

The simplest example with a nontrivial topology is when Ξ is equivalent to the circle and τ_1 is the translation by a fixed θ, as in the examples from Figs. 3 and 4. For $N = 1$, we know from the ordinary Fourier analysis that the algebra $C(\Xi)$ is generated by one function, $v(s) = e^{is}$, where s is the coordinate along the Ξ, assumed to be a closed loop of length 2π. The commutation relations can be computed (18) explicitly:

$$v\,u = u\,(v \circ \tau_1) = e^{i\theta} u\, v, \tag{25}$$

because $(v \circ \tau_1)(s) = e^{i(s+\theta)} = e^{i\theta} v(s)$. The conclusion is that $\mathcal{A}$ is the noncommutative two-torus. This algebra is the same as the one generated by the magnetic translations, from where one draws the Hamiltonians for electrons hopping on a lattice in a perpendicular uniform magnetic field. The latter is the setting where the integer quantum Hall effect (IQHE) is observed, which is the prototypical topological system from class A in two dimensions. As we shall see, there are extremely close spectral and topological similarities between those systems and the ones studied in this work.

One important point of these exercises was to convey that if (Ξ, τ) can be resolved and is simple enough, then the algebra $\mathcal{A}$ can be computed explicitly. In many cases, it can be connected with already well-studied algebras. In these cases, the classification of the gapped Hamiltonians can be fully carried out and the bulk-boundary principle can be formulated very precisely, as we shall see next.

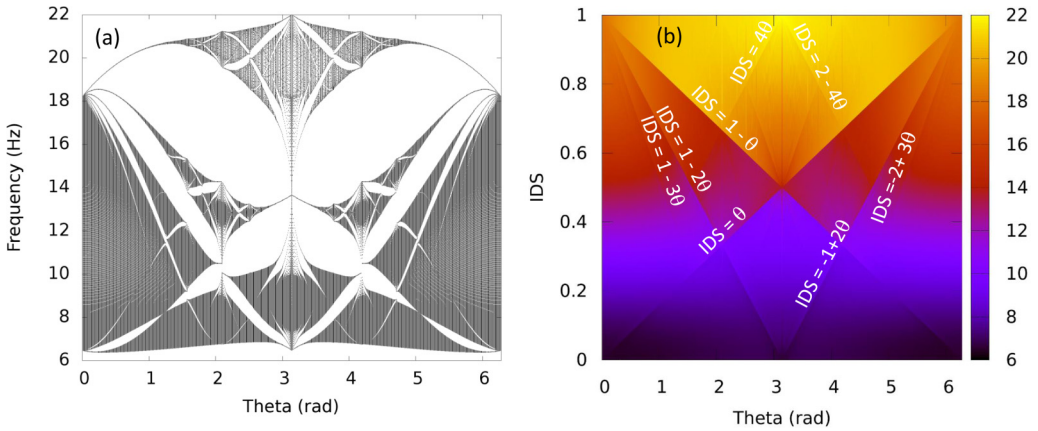

FIG. 5. Bulk spectral characteristics of the Hamiltonian (9) over the pattern from Fig. 3. (a) Bulk spectrum as function of parameter θ. The parameters l_0 and r have been fixed to the experimental values (see Fig. 6). (b) Integrated density of states (26) rendered as function of θ and frequency. The frequency axis is out of the plane.

IV. DECIPHERING THE BULK

A. Facts and observations

The resonant frequency spectrum for Hamiltonian (9) over the pattern (16) is shown in Fig. 5(a) as function of θ. The calculation was performed on a finite pattern of length $L = 840$ with periodic boundary condition for all commensurate values $\theta_n = \frac{2n\pi}{L}$ (note that the spectrum is known to be continuous of θ, hence the use of rational values is not an issue here). The empirical couplings α and β have been used in these calculations. The similarity between this spectrum and the Hofstadter spectrum [30] is remarkable. The main characteristic of the spectrum is the fractal network of spectral gaps. Despite its complexity, the spectral gaps can be labeled uniquely by just two integer numbers [31]. A practical way to achieve this labeling is to compute the integrated density of states (IDS), defined as

$$\mathrm{IDS}(f) = \left.\frac{\text{no. resonant frequencies below } f}{\text{Length } L}\right|_{L\to\infty}. \quad (26)$$

A graphic representation of IDS as a function of f and θ is reported in Fig. 5(b), as derived from the data reported in Fig. 5(a). In this rendering, the sharp changes in color are associated with the spectral gaps and the value of IDS inside the spectral gaps are all characterized by straight lines:

$$\mathrm{IDS}(\theta) = n + m\,\frac{\theta}{2\pi}, \quad n, m \in \mathbb{Z}. \quad (27)$$

Another key observation is that, since $N = 1$, the IDS is always bound to the interval $[0, 1]$. As we shall see later, the index m in (27) is the topological number which dictates the presence or absence of edge modes. Examining (27), one sees that there are only two instances where $m = 0$; when the states are fully depopulated (IDS $= 0$) or fully populated (IDS $= 1$). We can now anticipate the main finding of our work; every gap seen in Fig. 5(a) is topological in the sense that $m \neq 0$ and this implies the emergence of topological edge states. This is a statement which applies to any Hamiltonian (14) with $N = 1$. Thus, it is an intrinsic characteristic of the pattern. By all measures, the pattern can be called topological.

The bulk spectrum has been mapped experimentally for select values of θ. The setup is shown in Figs. 6(a) and 6(b). Throughout, the units of length are millimeters. To accommodate for the diameter, $D = 66$ mm, of the spinners, their centers have been arranged according to the algorithm $x_n = 76n + 2\,\sin(n\theta)$, $\theta = \frac{6\pi}{32}$, leading to a distance between the magnets [see Eq. (6)]:

$$d_n = 10 + 2\sin[(n+1)\theta] - 2\sin(n\theta), \quad n \in \mathbb{Z}. \quad (28)$$

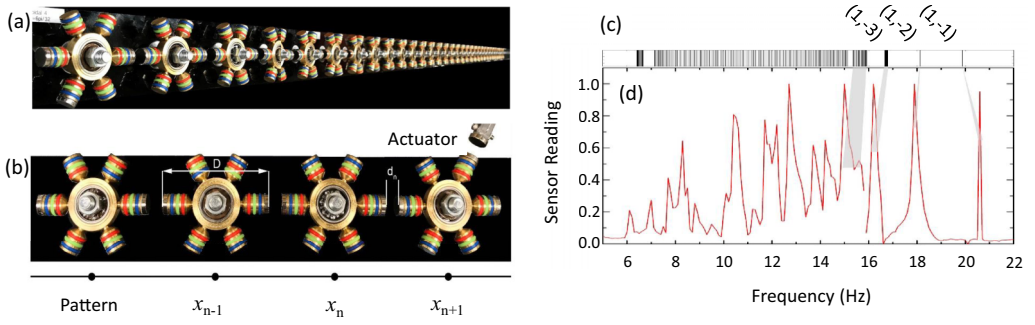

FIG. 6. Experimental bulk spectral characteristics. (a) A system of 32 spinners arranged in pattern (16). (b) Notations and experimental values: $\theta = \frac{6\pi}{32}$, $D = 66$ mm, $l_0 = 76$ mm, $r = 2$ mm. (c) Theoretically computed bulk spectrum for $\theta = \frac{2\pi}{\sqrt{117}} = \frac{6\pi}{32} + \mathcal{O}(10^{-3})$, together with the gap labels for the upper gaps, as extracted from Fig. 5. (d) Experimental reading from an accelerometer placed in the bulk of the system. The correspondence between theory and experiment is shown by the shaded regions.

These are the inputs for Hamiltonian (9). The theoretically computed spectrum and the experimentally measured one are reported in Figs. 6(c) and 6(d), respectively. The overall quantitative agreement is good, especially for the upper part of the spectrum. In fact, a rigorous correspondence between the two was established [see the guiding shaded regions in Figs. 6(c) and 6(d)], by matching the experimental and theoretical profiles of the normal modes. The IDS is extremely difficult to map experimentally since the size of the system needs to be appreciable and each of the resonant frequencies needs to be resolved. For these reasons, no attempt was made towards an experimental measurement.

B. Gap labeling: *K*-theoretic account

One extremely puzzling question is how do the straight lines emerge in Fig. 5(b), given that no tuning of the coupling coefficients has been attempted? For example, identical straight lines will show up even if the spinners are arranged in the complicated pattern shown in Fig. 4. The fundamental principle behind this phenomenon is easily explained by the K theory of the observables algebra, $\mathcal{A}$ [31].

Given an element h of the C^* algebra and a continuous function $\varphi : \mathbb{C} \to \mathbb{C}$, one can define a functional calculus $\varphi(h)$ by approximating φ by polynomials and taking the limit with respect to (21). This limit exists if and only if φ is continuous on the spectrum of h (see [58]). The example which will often appear from now on is the gap projection $p_G = \chi_{(-\infty,G]}(h)$, where h is the element of $\mathcal{A}$ which generates a covariant family of gapped Hamiltonians (H_ω, G). From now on, G will represent the gap itself and also an arbitrary point from the gap. Also, χ is the characteristic function of the specified interval. In the expression of p_G, $\chi_{(-\infty,G]}$ has a discontinuity at G but, since it occurs outside the spectrum of h, p_G is indeed an element of $\mathcal{A}$, which generates the spectral projections of H_ω's onto the spectrum below G. Consider now the family of functions $\varphi_t(x) = \frac{x-G}{1-t+t|x-G|}$, which interpolates continuously between $\varphi_0(x) = x$ and $\varphi_1(x) = \mathrm{sgn}(x-G)$. Then, $\varphi_t(H_\omega)$ interpolates continuously between H_ω and $\mathrm{sgn}(H_\omega) = 1 - 2\chi_{(-\infty,G]}(H_\omega)$. What this suggests is that classifying gap Hamiltonians (H_ω, G) are the same as classifying the projections $P_\omega(G) = \chi_{(-\infty,G]}(H_\omega)$ or, at the level of algebra $\mathcal{A}$, the projections p_G. Typically, there are many projections in an algebra but, if they are organized in topological equivalence classes, their accountability becomes possible. This is what K theory offers [25,59–62].

Given a generic C^* algebra $\mathcal{A}$, the K_0 group is defined as the classes $[p]_0$ of projections (i.e., $p^2 = p^* = p$) from $M_N(\mathbb{C}) \otimes \mathcal{A}$ with N arbitrarily large [hence $M_\infty(\mathbb{C})$ is used instead], where two projections belong to the same class iff they can be continuously deformed into each other or if there is $u \in M_\infty(\mathbb{C}) \otimes \mathcal{A}$ such that $p' = upu^*$ [when $\mathcal{A}$ is tensored by $M_\infty(\mathbb{C})$, the two criterion coincide]. Given two projections and their classes, one defines

$$[p]_0 \oplus [q]_0 = \begin{pmatrix} p & 0 \\ 0 & q \end{pmatrix}_0,$$

which makes K_0 into an Abelian semigroup, which then can be completed to a group. This is how $K_0(\mathcal{A})$ group is defined. Similarly, two unitary elements from $M_\infty(\mathbb{C}) \otimes \mathcal{A}$ are declared to be in the same K_1 class if they can be continuously deformed into each other. Given two unitaries and their K_1 classes, one defines the binary operation $[u]_1 \odot [u']_1 = [uu']_1$, which transforms $K_1(\mathcal{A})$ into an Abelian group. Since the projections and unitaries are drawn from $M_\infty(\mathbb{C}) \otimes \mathcal{A}$, we can simplify and take $N = 1$ in the definition of the bulk algebra, because $M_\infty(\mathbb{C})$ automatically takes care of the internal degrees of freedom!

We now state a central statement. By definition, the class of a projection is a topological invariant, though not a numerical one. As long as we classify the systems by K theory, which is now well understood within our community to be the physically correct way (see next paragraph), the class $[p_G]_0$ inside the K_0 group is the most general topological invariant that can be associated to a gap projection. Another key observation is that, if $\mathcal{A}$ is a separable C^* algebra as in our case, then both $K_0(\mathcal{A})$ and $K_1(\mathcal{A})$ are, at most, countable. In fact, for the noncommutative two-torus, which is the algebra associated to our patterns, $K_0(\mathcal{A}) \simeq \mathbb{Z}^2$, hence it has only two generators, the identity $[1]_0$ and the Rieffel projection $[p_\theta]_0$ [63]. As such, up to homotopies, any projection from $M_\infty(\mathbb{C}) \otimes \mathcal{A}$ can be decomposed as

$$[p]_0 = [1]_0 \oplus \cdots \oplus [1]_0 \oplus [p_\theta]_0 \oplus \cdots \oplus [p_\theta], \tag{29}$$

or simply as

$$[p]_0 = n\,[1]_0 + m\,[p_\theta]_0, \quad n, m \in \mathbb{Z}. \tag{30}$$

Therefore, we can locate p in $K_0(\mathcal{A})$ using just the two integers n and m. As long as one classifies by K theory, these integers represent the complete set of topological invariants that can be associated to a projection. It remains to show that they are the same numbers appearing in our previous IDS analysis. For this, note that the IDS values inside the gaps can be also computed as the trace per length of the gap projections:

$$\mathrm{IDS}(G) = \lim_{N\to\infty} \frac{1}{2N} \sum_{n=-N}^{N} \langle n|P_\omega(G)|n\rangle. \tag{31}$$

At the level of algebra $\mathcal{A}$, the trace per length has a very simple interpretation. Indeed,

$$\begin{aligned} \lim_{N\to\infty} \frac{1}{2N} \sum_{n=-N}^{N} \langle n|A_\omega|n\rangle &= \lim_{N\to\infty} \frac{1}{2N} \sum_{n=-N}^{N} \langle n|\pi_\omega(a)|n\rangle \\ &= \lim_{N\to\infty} \frac{1}{2N} \sum_{n=-N}^{N} a_0(\tau_n\omega), \end{aligned} \tag{32}$$

and, by using Birkhoff's ergodic theorem [64], we can conclude that

$$\lim_{N\to\infty} \frac{1}{2N} \sum_{n=-N}^{N} \langle n|A_\omega|n\rangle = \int_\Xi d\mathbb{P}(\omega)\, a_0(\omega), \tag{33}$$

where $\mathbb{P}(\omega)$ is the unique translation invariant probability measure on $\mathbb{S}^1$. The right-hand side defines a trace on the algebra $\mathcal{A}$, which will be denoted by $\mathcal{T}$, i.e., a positive linear functional such that $\mathcal{T}(aa') = \mathcal{T}(a'a)$ for any $a, a' \in \mathcal{A}$. This trace can be trivially extended over $M_\infty(\mathbb{C}) \otimes \mathcal{A}$ by tensoring with the ordinary trace. Now, consider p and p' from the same K_0 class. Then there exists u such that $p' = upu^*$ and

consequently $\mathcal{T}(p) = \mathcal{T}(p')$. As a consequence, the trace $\mathcal{T}$ is constant over the topological classes, hence it defines a topological invariant. Given the linearity of the trace [25,31]:

$$\begin{aligned}\mathrm{IDS}(G) &= \mathcal{T}([p_G]_0) = \mathcal{T}(n[1]_0 \oplus m[p_\theta]_0)\\ &= n\mathcal{T}([1]_0) + m\mathcal{T}([p_\theta]_0) = n + m\theta, \end{aligned} \quad (34)$$

where for the last equality we used the fundamental result $\mathcal{T}(p_\theta) = \theta$ [63].

Several observations are in place, with fundamental consequences for experiments. Given any Hilbert space $\mathcal{H}$, its algebra $\mathbb{B}(\mathcal{H})$ of bounded operators is not separable and its K theory is irrelevant. In fact $K_0(\mathbb{B}) = 0$ for any separable $\mathcal{H}$ [60]), so it is very important that all the Hamiltonians over a pattern can be all drawn from the smaller algebra $\mathcal{A}$ with a nontrivial K theory. The number of internal degrees of the resonators cannot be fixed in general. For example, in quantum chemistry we use pseudopotentials and discard the deep electron states, which are chemically inert, and we also get rid of the states in the continuum spectrum. The tight-binding Hamiltonians used to model topological insulators are just effective Hamiltonians where an infinite number of internal states are "integrated out." It is important to acknowledge that, in K theory, states can be added without changing the classification. This is why the K-theoretic classification is more physical than any other classification schemes. Now an extremely fine and important point: by definition, the labels n and m cannot be changed as long as p is continuously deformed. This deformation needs to happen inside the algebra $\mathcal{A}$ by either deforming the resonators, the way they couple, or by deforming the pattern without changing the topology of the discrete hull Ξ (as for the patterns in Figs. 3 and 4). These give the precise experimental conditions in which the predictions based on K theory will hold, something which in the physical literature are completely overlooked, yet they are paramount for the practical applications.

V. TOPOLOGICAL EDGE STATES

In this section, we remove the degrees of freedom with index $n < 0$ and examine the spectral properties of the edged Hamiltonians, like

$$\widehat{H}_\omega = \sum_{n,n'\geqslant 0} w_{n,n'}(\omega) \otimes |n\rangle\langle n'|, \quad (35)$$

defined over the Hilbert space $\mathbb{C}^N \otimes \ell^2(\mathbb{N})$. The above Hamiltonians assume that all spinners with $n < 0$ have been jammed. However, the edge can be generated in many different ways. For example, one could remove all the spinners with index $n < 0$, in which case some of the coupling coefficients near the edge are altered. In real-world applications, we may never produce and maintain clean edges. Instead, the coupling constants will be drastically affected near the edge by the cutting process or by gradual wear and tear. Hence, it is very important to produce statements that are independent of the boundary conditions. This is another aspect where K theory shows its effectiveness.

When a bulk system H_ω is edged to $\widehat{H}_\omega$, the bulk spectrum remains in place, but an additional spectrum can emerge inside the bulk spectral gaps. It is useful to introduce the edge spectrum as

$$\mathrm{Spec}_e(\widehat{H}_\omega) = \mathrm{Spec}(\widehat{H}_\omega) \setminus \mathrm{Spec}(H_\omega). \quad (36)$$

In one- and quasi-one-dimensional systems, $\mathrm{Spec}_e(\widehat{H}_\omega)$ can only contain a finite number of eigenvalues. Interesting things can happen when the systems are stacked as

$$\widehat{H} = \bigoplus_{\omega\in\Omega} \widehat{H}_\omega. \quad (37)$$

The bulk spectrum remains unchanged, but the edge spectrum now consists of

$$\mathrm{Spec}_e(\widehat{H}) = \bigcup_{\omega\in\Xi} \mathrm{Spec}_e(\widehat{H}_\omega) = \overline{\bigcup_{a\in\mathbb{Z}} \mathrm{Spec}_e(\widehat{H}_{\tau_a\omega})}, \quad (38)$$

where in the last equality we used the fact that the orbit of ω is dense in Ξ. The last equality shows that the stacking can be achieved by simply cutting the same chain but at different locations. The edge spectrum is said to be topological if it fills the bulk gap completely:

$$\mathrm{Spec}_e(\widehat{H}) \cap G = G, \quad (39)$$

and if it cannot be removed by any adiabatic deformation of the bulk system or by changing the boundary condition.

A. Facts and observations

After removing all the spinners with index $n < 0$, the dynamics is described by the Hamiltonian

$$\begin{aligned}\widehat{H}_\omega = \sum_{n\in\mathbb{N}} \{&[\alpha(d_{n-1}) + \alpha(d_n)]|n\rangle\langle n|\\ &+ \beta(d_{n-1})|n\rangle\langle n-1| + \beta(d_n)|n\rangle\langle n+1|\}, \end{aligned} \quad (40)$$

with the understanding that $\alpha(d_{-1}) = \beta(d_{-1}) = 0$. In Fig. 7 we show the theoretically computed spectra of N_s stackings of edged systems,

$$\bigcup_{a=0,\ldots,N_s-1} \mathrm{Spec}(\widehat{H}_{\tau_a\omega}), \quad N_s = 1,\ 10,\ 100,\ 1000, \quad (41)$$

for the pattern (28) with the experimental coupling coefficients. The angle was fixed at $\theta = \frac{2\pi}{\sqrt{117}} \approx 0.5808$. This particular irrational fraction of 2π accepts a good rational approximation $\theta = \frac{6\pi}{32} + \mathcal{O}(10^{-3})$ and is used in the experiment. In the numerical calculations the exact θ was used and the calculation was performed on a finite pattern with $L = 7669$, chosen based on the rational approximation $\theta = 2\pi\frac{709}{7669} + \mathcal{O}(10^{-7})$. This ensures that all graphical representations in Fig. 7 are extremely accurate.

Figure 7(a) reports the computed IDS together with the gap labels (n, m) derived from the values of IDS inside the gaps. They are in agreement with the labels seen in Fig. 5. Examining Figs. 7(b)–7(e), one can witness how all the spectral gaps of the bulk Hamiltonian are gradually filled with boundary spectrum as more systems are added to the stack. The resulting bundle of systems is topological in the sense described above, in full agreement with the gap labels. The edge spectrum can be resolved asa function of $\omega \in \mathbb{S}^1$ as in Fig. 8, by noticing that the coordinate of $\tau_a\omega$ on the circle is the angle $a\theta$. The simulation in panel (a) shows that the edge spectrum splits into chiral bands, whose number equals the gap label m. Since the

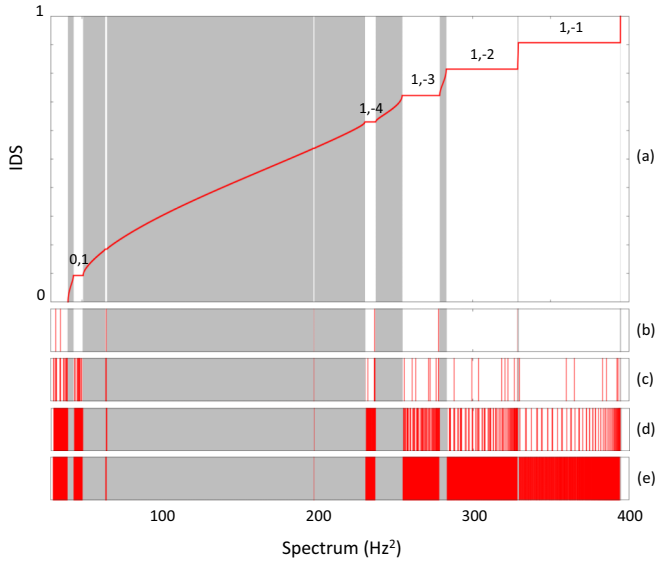

FIG. 7. Numerical illustration of the topological edge spectrum. (a) Integrated density of states (IDS) for the pattern (28) with $\theta = \frac{2\pi}{\sqrt{117}}$ (red curve). Overlaid in gray is the bulk spectrum. The IDS values $n + m\theta$ inside the spectral gaps are indicated by the pairs of integers (n, m). (b)–(e) Edge spectrum (red marks) of N_s stacked edged systems, with $N_s = 1, 10, 100, 1000$, respectively. For convenience, the bulk spectrum is shown in gray.

computation was performed on a finite rather than a halved system, the chiral bands appear always in pairs, one per edge.

The edge spectrum has been reproduced experimentally as reported in Fig. 8(b). In these experiments, the system shown in Fig. 6(a) is actuated from the first spinner between 14 and 21 Hz in steps of 0.1 Hz. One spinner was then moved from the front to the back of the chain, effectively implementing the translation $\tau_1\omega$, and the measurements were repeated. By cycling this whole process, one can shift the pattern 32 times and generate the experimental measure of the edge spectrum (38). Topological edge modes are detected at proper

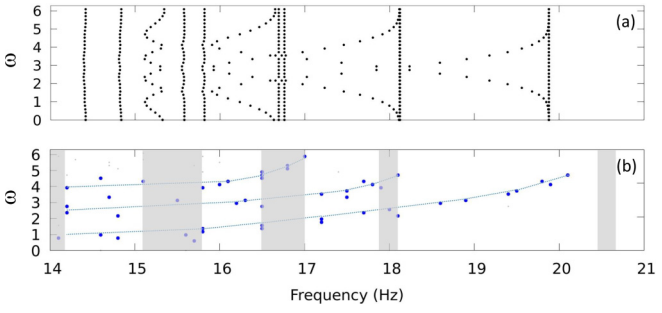

FIG. 8. Theoretical edge spectrum vs the measured one. (a) The predicted theoretical spectrum of a chain of 32 spinners with free ends, mapped as function of ω. (b) The resonant frequencies (dots) recorder at one end of the chain, with the bulk spectrum from Fig. 6(d) indicated by vertical grey bars. Dotted lines have been added to help indicate the chiral bands. In both panels, ω runs over the experimentally available values $\omega_n = n\theta$, $n = 0, \ldots, 31$. Note that the theoretical plots include both (left and right) edge modes and this is why the chiral bands come in pairs.

frequencies inside the bulk spectral gaps as the frequency is swept. They manifest as extremely strong and well-defined resonances, visible to the naked eye. A quantitative account of this phenomenon is reported in Fig. 9, which displays the reading from an accelerometer placed on the arm of the second spinner from the edge. Figure 10 resolves the spatial profile of an edge resonant mode detected in the last and most prominent bulk gap. It confirms that the mode is extremely well localized near the edge.

Last, in the Supplemental Material [65] we report video recordings of the response of the experimental system when actuating from one end at different frequencies. In these experimental observations, the system has been enlarged to 64 spinners and the chain has been wrapped around in a spiral-like configuration. Since the excitations along the chain caries only angular and no linear momentum, there is no backscattering at the sharp corners. Another way of seeing this is by observing that the equations of motion remain unchanged. The first video recording exemplifies a bulk mode, where one can see a standing-wave pattern over the entire structure, even when the system is actuated only at one end. In the second recording, the frequency has been tuned on the topological resonant mode occurring in the last spectral gap. To exemplify the difference between this resonant response and a trivial forced oscillation, we report a third recording where the driving frequency is off resonance.

B. Algebra of half-space observables

For the half space, the shift operator, which on the new Hilbert space will be called $\widehat{S}$, is no longer unitary, but instead

$$\widehat{S}\,\widehat{S}^* = I, \quad \widehat{S}^*\,\widehat{S} = I - P_0, \quad P_0 = |0\rangle\langle 0|. \tag{42}$$

This suggests the definition of the half-space algebra $\widehat{\mathcal{A}}$ as the algebra generated by $C_N(\Xi)$ and the operator $\hat{u}$ satisfying the same commutation relations (18). However, $\hat{u}^*\hat{u} = 1 - \hat{e}$, with $\hat{e}$ a proper projection $\hat{e}^2 = \hat{e}^* = \hat{e} \neq 1$. The half-space algebra accepts the following canonical representation:

$$C_N(\Xi) \ni f \to \hat{\pi}_\omega(f) = \sum_{n\geqslant 0} f(\tau_n\omega) \otimes |n\rangle\langle n|, \tag{43}$$

and $\hat{\pi}_\omega(\hat{u}) = \widehat{S}$, which generates all half-space physical Hamiltonians [27]. In general, we have the isomorphism of algebras $\widehat{\mathcal{A}} \simeq \bigoplus_{\omega\in\Xi} \hat{\pi}_\omega(\widehat{\mathcal{A}})$ hence

$$\mathrm{Spec}(\hat{h}) = \bigcup_{\omega\in\Xi} \mathrm{Spec}(H_\omega) = \overline{\bigcup_{a\in\mathbb{Z}} \mathrm{Spec}(H_{\tau_a\omega})} = \mathrm{Spec}(\widehat{H}), \tag{44}$$

with H from (37). In other words, the spectrum of $\hat{h}$ coincides with the spectrum of the stacked systems introduced and discussed above. This is important to keep in mind because the K-theoretic bulk-boundary principle contains a statement about the spectrum of $\hat{h}$, hence of the stacked systems, as already highlighted in Fig. 7.

Inside $\widehat{\mathcal{A}}$, there is the ideal $\widetilde{\mathcal{A}}$ made up of elements of the form $\hat{a}\,\hat{e}\,\hat{b}$ for some $\hat{a}, \hat{b} \in \widehat{\mathcal{A}}$. When represented on the physical space, such elements are localized near the boundary, hence $\widetilde{\mathcal{A}}$ is called the boundary algebra [27]. Given a bulk Hamiltonian h, the half-space Hamiltonian with Dirichlet

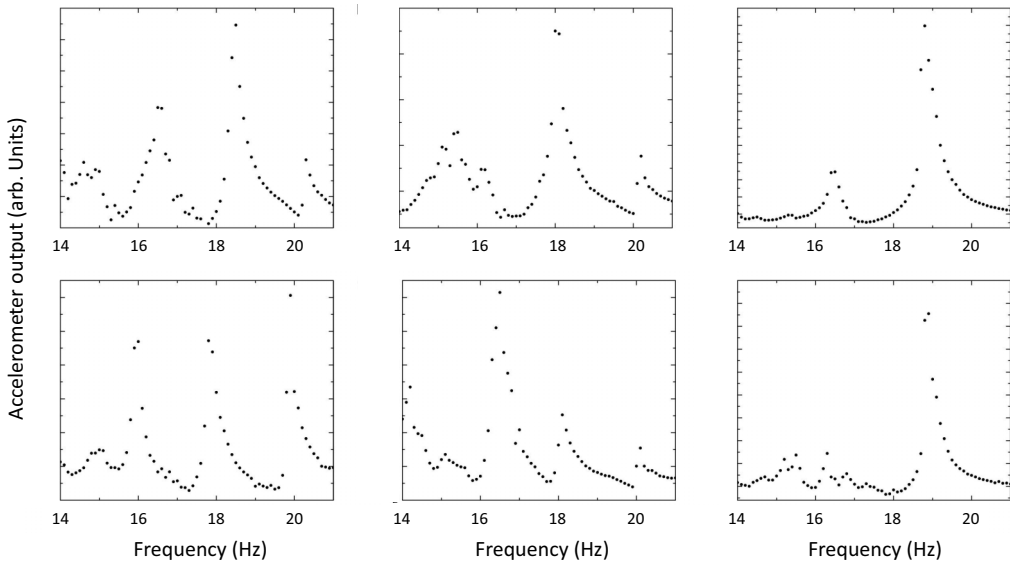

FIG. 9. Measurements of the edge resonances. The panels report the readings from accelerometers placed on the second spinner from the edge for randomly rotated configurations of the spinner chain. The edge resonances appear as prominent peaks in these measurements.

boundary condition, i.e., all couplings crossing the boundary set to zero, is generated by

$$\hat{h}_D = \sum_{q\geqslant 0} h_q \hat{u}^q + \sum_{q<0} h_q (\hat{u}^*)^{|q|}.$$

By adding elements from $\widetilde{\mathcal{A}}$, $\hat{h} = \hat{h}_D + \tilde{h}$, the Dirichlet can be changed into any other boundary condition, hence the formalism is completely general. An important relation established in [27] is the isomorphisms between $\widetilde{\mathcal{A}}$ and $M_\infty(\mathbb{C}) \otimes C(\Xi)$, which will play an important role for the bulk-boundary correspondence principle. That is because then $K_*(\widetilde{\mathcal{A}}) = K_*[C(\Xi)]$, and since $\Xi \simeq \mathbb{S}^1$, $K_*(\widetilde{\mathcal{A}}) \simeq \mathbb{Z}$. In particular, $K_1(\widetilde{\mathcal{A}})$ is generated by $[v]_1$, with v introduced in (25).

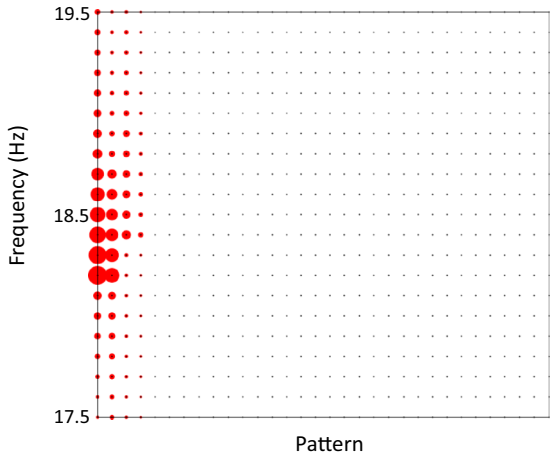

FIG. 10. Spatial profile of a resonant mode. The data report the readings from four accelerometers placed on the first four spinners from the edge, as the frequency was swept over the last and most prominent bulk gap. The amplitudes of these readings are proportional with the size of the disks. For convenience, the full pattern of spinners is also shown.

C. Engine of the bulk-boundary correspondence

The following exact sequence between the algebras of physical observables is well established [26,27]:

$$0 \longrightarrow \widetilde{\mathcal{A}} \xhookrightarrow{\ i\ } \widehat{\mathcal{A}} \xrightarrow{\ \mathrm{ev}\ } \mathcal{A} \longrightarrow 0, \tag{45}$$

with $\mathrm{ev}(\hat{u}) = u$. This exact sequence sets in motion a six-term exact sequence at the K-theory level [60–62]:

$$\begin{array}{ccccc} K_0(\widetilde{\mathcal{A}}) & \xrightarrow{\ i_*\ } & K_0(\widehat{\mathcal{A}}) & \xrightarrow{\ \mathrm{ev}_*\ } & K_0(\mathcal{A}) \\ \uparrow{\scriptstyle \mathrm{Ind}} & & & & \downarrow{\scriptstyle \mathrm{Exp}} \\ K_1(\mathcal{A}) & \xleftarrow{\ \mathrm{ev}_*\ } & K_1(\widehat{\mathcal{A}}) & \xleftarrow{\ i_*\ } & K_1(\widetilde{\mathcal{A}}) \end{array} \tag{46}$$

The relevance of this diagram to the bulk-boundary principle program was established by the work of [26]. Examining the right side of the diagram, one can see the standard K-theory map Exp taking projections from the bulk algebra into unitaries from the boundary algebras. Given a gapped bulk Hamiltonian (h, G) from $\mathcal{A}$, one defines a function $\phi : \mathbb{R} \to \mathbb{R}$ with a sharp, but continuous, variation in an ϵ interval around any point G inside the gap, such that $\phi = 0/1$ below/above that interval. Besides these requirements, ϕ is completely arbitrary. If $\hat{h}$ is any half-space Hamiltonian obtained from h, i.e., $\mathrm{ev}(\hat{h}) = h$, then [26,27]

$$\mathrm{Exp}[p_G]_0 = [\tilde{u}_G]_1, \quad \tilde{u}_G = e^{2\pi i \phi(\hat{h})}. \tag{47}$$

As the notation suggests, $\tilde{u}_G$ is a unitary element of the boundary algebra $\widetilde{\mathcal{A}}$, because the function $e^{2\pi\epsilon} - 1$ is nonzero only on the edge spectrum. Hence, $e^{2\pi\hat{h}} - 1$ is built only from boundary states. If the half-space Hamiltonian $\hat{h}$ is gapped, then we can take G and the variation of the function ϕ inside this gap, in which case ϕ is either 0 or 1 on the spectrum of $\hat{h}$. By the rules of functional calculus, $\tilde{u}_G$ is the identity. If

$\hat{h}$ is gapped, then $[p_G]_0$ is necessarily mapped into the trivial K_1 class $[1]_1$ by the Exp map. However, if the latter is not the case, then $\hat{h}$ cannot be gapped. The key conclusion is that if $\mathrm{Exp}[p_G]_0 \neq [1]_1$, then the topological boundary spectrum emerges, filling the *entire* bulk gap. This spectrum cannot be gapped by any boundary condition or adiabatic deformation of h.

To summarize, in order to establish a bulk-boundary correspondence principle, one needs to resolve the K theories of both bulk and boundary algebras, as well as the action of the Exp map on the generators of $K_0(\mathcal{A})$. We should warn the reader that just the condition $[p_G]_0 \neq [0]_0$ is in general not enough, a counterexample being the case of Fibonacci patterns where the whole K_0 group is mapped by the Exp map into the trivial K_1 class of the boundary [47].

D. Topological patterns, indeed

From the bulk analysis, we know that $K_0(\mathcal{A})$ is generated by $[1]_0$ and $[e_\theta]_0$ and that every bulk gap projection accepts a decomposition:

$$[p_G]_0 = n\,[1]_0 + m\,[e_\theta]_0, \quad m \neq 0. \tag{48}$$

The action of the Exp map is also known [27] explicitly:

$$\mathrm{Exp}[1]_0 = [1]_1, \quad \mathrm{Exp}[e_\theta]_0 = [v]_1. \tag{49}$$

One can see that any gap projection is mapped nontrivially:

$$\mathrm{Exp}[p_G]_0 = m\,[v]_1 \neq [1]_1, \tag{50}$$

and, consequentially, the topological edge spectrum fills every single spectral gap of a bulk Hamiltonian, regardless of its particular form. Furthermore, (50) automatically implies that $\tilde{u}_G$ is homotopic to v^m, hence m counts the winding of the eigenvalues of $\tilde{u}_G(\omega)$ as ω is varied along $\Xi \simeq \mathbb{S}^1$. In turn, this tells us that m counts the number of chiral edge bands of $\hat{h}$, in agreement with the observations from Fig. 8.

In the cases when there are more internal degrees of freedom, $N > 1$, the IDS will take values in the interval $[0, N-1]$, hence there are $N-1$ possible instances where m in (34) can be zero. As such, among the infinite number of bulk gaps there will be only $N-1$ gaps which are not topological, i.e., will not be filled with edge spectrum when the system is halved. If there is enough control over the design of metamaterials, of course, one should try to isolate just one degree of freedom per resonator but, if this is not possible, even the cases with large N's will still display plenty of topological gaps.

VI. DISCUSSION

We conclude with proposals of how our findings can be incorporated in practical applications. First, let us recall that the topological systems proposed here are fibers made of bundles of patterned chains H_ω, with ω sampling its configuration space. 1. As we have seen, this configuration space, which is the hull Ξ, can be sampled by simply shifting an infinite chain and this leads to the important observation that such bundles can be obtained by a simple and practical procedure. Indeed, by sequentially cutting equal pieces of length L from a single bulk sample and bundling these pieces together, one is effectively generating a fiber whose dynamics is described by $\bigoplus_{n\in\mathbb{N}} \hat{H}_{\tau_{nL}\omega}$ (provided L is large enough). Since $\tau_{nL}\omega$ is densely sampling the configuration space Ξ, the desired bundling has been achieved.

The bundle described above displays edge modes which cannot be removed by cutting, wear and tear, or by gentle bending of the strands. Additionally, the modes can be localized not only in space but also in frequency. By examining the spectral butterfly in Fig. 5, one can see that, by varying θ, one can align at least one bulk spectral gap at any desired frequency within the bulk range.

Let us end by noting that our conclusions are not bound to mechanical systems and they apply to any coupled resonators regardless of their nature. Hence, whenever spatial and frequency control over the excitation modes is desired, the proposed patterns can provide a convenient practical solution given the minimal tuning required.

[1] E. Prodan and C. Prodan, Topological Phonon Modes and their Role in Dynamic Instability of Microtubules, Phys. Rev. Lett. **103**, 248101 (2009).

[2] N. Berg, K. Joel, M. Koolyk, and E. Prodan, Topological phonon modes in filamentary structures, Phys. Rev. E **83**, 021913 (2011).

[3] L. Zhang, J. Ren, J.-S. Wang, and B. Li, The phonon hall effect: Theory and application, J. Phys.: Condens. Matter **23**, 305402 (2011).

[4] C. Kane and T. Lubensky, Topological boundary modes in isostatic lattices, Nat. Phys. **10**, 39 (2013).

[5] B.-G. Chen, N. Upadhyaya, and V. Vitelli, Nonlinear conduction via solitons in a topological mechanical insulator, Proc. Natl. Acad. Sci. USA **111**, 13004 (2014).

[6] A. B. Khanikaev, R. Fleury, S. H. Mousavi, and A. Alu, Topologically robust sound propagation in an angular-momentum-biased graphene-like resonator lattice, Nat. Commun. **6**, 8260 (2015).

[7] P. Deymier, K. Runge, N. Swinteck, and K. Muralidharan, Torsional topology and fermion-like behavior of elastic waves in phononic structures, C. R. Mec. **343**, 700 (2015).

[8] S. Mousavi, A. Khanikaev, and Z. Wang, Topologically protected elastic waves in phononic metamaterials, Nat. Commun. **6**, 8682 (2015).

[9] V. Peano, C. Brendel, M. Schmidt, and F. Marquardt, Topological Phases of Sound and Light, Phys. Rev. X **5**, 031011 (2015).

[10] J. Paulose, B.-G. Chen, and V. Vitelli, Topological modes bound to dislocations in mechanical metamaterials, Nat. Phys. **11**, 153 (2015).

[11] M. Xiao, W.-J. Chen, W.-Y. He, and C. Chan, Synthetic gauge flux and Weyl points in acoustic systems, Nat. Phys. **11**, 920 (2015).

[12] J. Paulose, A. Meeussen, and V. Vitelli, Selective buckling via states of self-stress in topological metamaterials, Proc. Natl. Acad. Sci. USA **112**, 7639 (2015).

[13] Y.-T. Wang, P.-G. Luan, and S. Zhang, Coriolis force induced topological order for classical mechanical vibrations, New J. Phys. **17**, 073031 (2015).

[14] M. Xiao, G. Ma, Z. Yang, P. Sheng, Z. Q. Zhang, and C. T. Chan, Geometric phase and band inversion in periodic acoustic systems, Nat. Phys. **11**, 240 (2015).

[15] X. Mao, A. Souslov, C. Mendoza, and T. Lubensky, Mechanical instability at finite temperature, Nat. Commun. **6**, 5968 (2015).

[16] T. Kariyado and Y. Hatsugai, Manipulation of Dirac cones in mechanical graphene, Sci. Rep. **5**, 18107 (2015).

[17] L. M. Nash, D. Kleckner, A. Read, V. Vitelli, A. M. Turner, and W. T. M. Irvine, Topological mechanics of gyroscopic metamaterials, Proc. Natl. Acad. Sci. USA **112**, 14495 (2015).

[18] R. Süsstrunk and S. Huber, Observation of phononic helical edge states in a mechanical topological insulator, Science **349**, 47 (2015).

[19] R. Süsstrunk and S. D. Huber, Classification of topological phonons in linear mechanical metamaterials, Proc. Natl. Acad. Sci. USA **113**, E4767 (2016).

[20] P. Deymier and K. Runge, One-dimensional mass-spring chains supporting elastic waves with non-conventional topology, Crystals **6**, 44 (2016).

[21] R. Pal, M. Schaeffer, and M. Ruzzene, Helical edge states and topological phase transitions in phononic systems using bi-layered lattices, J. Appl. Phys. **119**, 084305 (2016).

[22] G. Salerno, T. Ozawa, H. Price, and I. Carusotto, Floquet topological system based on frequency-modulated classical coupled harmonic oscillators, Phys. Rev. B **93**, 085105 (2016).

[23] D. Z. Rocklin, B. Gin–ge Chen, M. Falk, V. Vitelli, and T. C. Lubensky, Mechanical Weyl Modes in Topological Maxwell Lattices, Phys. Rev. Lett. **116**, 135503 (2016).

[24] E. Prodan, K. Dobiszewski, A. Kanwal, J. Palmieri, and Camelia Prodan, Dynamical Majorana edge modes in a broad class of topological mechanical systems, Nat. Commun. **8**, 14587 (2017).

[25] J. Bellissard, K-theory of C*-algebras in solid state physics, in *Lecture Notes in Physics*, edited by T. Dorlas, M. Hugenholtz, and M. Winnink (Springer-Verlag, Berlin, 1986), Vol. 257, pp. 99–156.

[26] J. Kellendonk, T. Richter, and H. Schulz-Baldes, Edge current channels and Chern numbers in the integer quantum Hall effect, Rev. Math. Phys. **14**, 87 (2002).

[27] E. Prodan and H. Schulz-Baldes, *Bulk and Boundary Invariants for Complex Topological Insulators: From K-theory to Physics* (Springer, Berlin, 2016).

[28] E. Prodan and Y. Shmalo, The K-theoretic bulk-boundary principle for dynamically patterned resonators, J. Geom. Phys. **135**, 135 (2019).

[29] M. C. Kreisel, Gabor frames for quasicrystals and K-theory, Ph.D. thesis, University of Maryland, 2015.

[30] D. R. Hofstadter, Energy levels and wave functions of Bloch electrons in rational and irrational magnetic fields, Phys. Rev. B **14**, 2239 (1976).

[31] J. Bellissard, Gap labeling theorems for Schroedinger operators, in *From Number Theory to Physics*, edited by M. Waldschmidt, P. Moussa, J.-M. Luck, and C. Itzykson (Springer, Berlin, 1995).

[32] Y. E. Kraus, Y. Lahini, Z. Ringel, M. Verbin, and O. Zilberberg, Topological States and Adiabatic Pumping in Quasicrystals, Phys. Rev. Lett. **109**, 106402 (2012).

[33] M. Verbin, O. Zilberberg, Y. E. Kraus, Y. Lahini, and Y. Silberberg, Observation of Topological Phase Transitions in Photonic Quasicrystals, Phys. Rev. Lett. **110**, 076403 (2013).

[34] K. A. Madsen, E. J. Bergholtz, and P. W. Brouwer, Topological equivalence of crystal and quasicrystal band structures, Phys. Rev. B **88**, 125118 (2013).

[35] E. Prodan, Virtual topological insulators with real quantized physics, Phys. Rev. B **91**, 245104 (2015).

[36] Y. E. Kraus, Z. Ringel, and O. Zilberberg, Four-Dimensional Quantum Hall Effect in a Two-Dimensional Quasicrystal, Phys. Rev. Lett. **111**, 226401 (2013).

[37] W. Hu, J. C. Pillay, K. Wu, M. Pasek, P. P. Shum, and Y. D. Chong, Measurement of a Topological Edge Invariant in a Microwave Network, Phys. Rev. X **5**, 011012 (2015).

[38] Y. E. Kraus and O. Zilberberg, Topological Equivalence between the Fibonacci Quasicrystal and the Harper Model, Phys. Rev. Lett. **109**, 116404 (2012).

[39] D. Tanese, E. Gurevich, F. Baboux, T. Jacqmin, A. Lemaitre, E. Galopin, I. Sagnes, A. Amo, J. Bloch, and E. Akkermans, Fractal Energy Spectrum of a Polariton Gas in a Fibonacci Quasiperiodic Potential, Phys. Rev. Lett. **112**, 146404 (2014).

[40] D.-T. Tran, A. Dauphin, N. Goldman, and P. Gaspard, Topological Hofstadter insulators in a two-dimensional quasicrystal, Phys. Rev. B **91**, 085125 (2015).

[41] M. Verbin, O. Zilberberg, Y. Lahini, Y. E. Kraus, and Y. Silberberg, Topological pumping over a photonic Fibonacci quasicrystal, Phys. Rev. B **91**, 064201 (2015).

[42] E. Levy, A. Barak, A. Fisher, and E. Akkermans, Topological properties of Fibonacci quasicrystals : A scattering analysis of Chern numbers, arXiv:1509.04028.

[43] A. Dareau, E. Levy, M. B. Aguilera, R. Bouganne, E. Akkermans, F. Gerbier, and J. Beugnon, Revealing the Topology of Quasicrystals with a Diffraction Experiment, Phys. Rev. Lett. **119**, 215304 (2017).

[44] M. A. Bandres, M. C. Rechtsman, and M. Segev, Topological Photonic Quasicrystals: Fractal Topological Spectrum and Protected Transport, Phys. Rev. X **6**, 011016 (2016).

[45] F. Baboux, E. Levy, A. Lemaitre, C. Gómez, E. Galopin, L. L. Gratiet, I. Sagnes, A. Amo, J. Bloch, and E. Akkermans, Measuring topological invariants from generalized edge states in polaritonic quasicrystals, Phys. Rev. B **95**, 161114(R) (2017).

[46] A. Agarwala and V. B. Shenroy, Topological Insulators in Amorphous Systems, Phys. Rev. Lett. **118**, 236402 (2017).

[47] J. Kellendonk and E. Prodan, Bulk-Boundary Principle in Sturmian Kohmoto type models, arXiv:1710.07681.

[48] C. Bourne and E. Prodan, Non-commutative Chern numbers for generic aperiodic discrete systems, J. Phys. A: Math. Theor. **51**, 235202 (2018).

[49] N. P. Mitchell, L. M. Nash, D. Hexner, A. Turner, and W. T. M. Irvine, Amorphous topological insulators constructed from random point sets, Nat. Phys. **14**, 380 (2018).

[50] M. Lohse, C. Schweizer, H. M. Price, O. Zilberberg, and I. Bloch, Exploring 4D quantum hall physics with a 2D topological charge pump, Nature (London) **553**, 55 (2018).

[51] O. Zilberberg, S. Huang, J. Guglielmon, M. Wang, K. Chen, Y. E. Kraus, and M. C. Rechtsman, Photonic topological pumping through the edges of a dynamical four-dimensional quantum Hall system, Nature (London) **553**, 59 (2018).

[52] D. Zhou, L. Zhang, and X. Mao, Topological Edge Floppy Modes in Disordered Fiber Networks, Phys. Rev. Lett. **120**, 068003 (2018).

[53] A. P. Schnyder, S. Ryu, A. Furusaki, and A. W. W. Ludwig, Classification of topological insulators and superconductors in three spatial dimensions, Phys. Rev. B **78**, 195125 (2008).

[54] S. Ryu, A. P. Schnyder, A. Furusaki, and A. W. W. Ludwig, Topological insulators and superconductors: tenfold way and dimensional hierarchy, New J. Phys. **12**, 065010 (2010).

[55] A. Kitaev, Periodic table for topological insulators and superconductors, in *Advances in Theoretical Physics: Landau Memorial Conference*, AIP Conf. Proc. No. 1134, edited by Vladimir Lebedev and Mikhail Feigel'man (AIP, Melville, NY, 2009), p. 22.

[56] Y. Barlas and E. Prodan, Topological classification table implemented with classical passive metamaterials, Phys. Rev. B **98**, 094310 (2018).

[57] L. Sadun, *Topology of Tiling Spaces* (American Mathematical Society, Providence, 2008).

[58] W. Arveson, *A Short Course on Spectral Theory*, Graduate Texts in Mathematics Vol. 209 (Springer, Berlin, 2002).

[59] K. R. Davidson, C**-algebras by Example* (American Mathematical Society, Providence, RI, 1996).

[60] N. E. Wegge-Olsen, *K-theory and* C**-algebras* (Oxford University Press, Oxford, 1993).

[61] B. Blackadar, *K-theory for operator algebras*, Mathematical Sciences Research Institute Publications Vol. 5 (Cambridge University Press, Cambridge, UK, 1998).

[62] M. Rordam, F. Larsen, and N. Laustsen, *An Introduction to K-theory for* C**-algebras* (Cambridge University Press, Cambridge, UK, 2000).

[63] M. A. Rieffel, C^*-algebras associated with irrational rotations, Pac. J. Math. **93**, 415 (1981).

[64] G. D. Birkhoff, Proof of the ergodic theorem, Proc. Natl. Acad. Sci. USA **17**, 656 (1931).

[65] See Supplemental Material at http://link.aps.org/supplemental/10.1103/PhysRevMaterials.2.124203 for video recordings of the bulk and topological edge modes.